*mathematics*

MDPI

*Article*

# Detection of Current Transformer Saturation Based on Machine Learning

**Ismoil Odinaev [1], Andrey Pazderin [1], Murodbek Safaraliev [1], Firuz Kamalov [2,*], Mihail Senyuk [1] and Pavel Y. Gubin [1]**

[1] Department of Automated Electrical Systems, Ural Federal University, 620002 Yekaterinburg, Russia; a.v.pazderin@urfu.ru (A.P.); murodbek_03@mail.ru (M.S.); mdseniuk@urfu.ru (M.S.); pavel.gubin@urfu.ru (P.Y.G.)
[2] Department of Electrical Engineering, Canadian University Dubai, Dubai 117781, United Arab Emirates
* Correspondence: firuz@cud.ac.ae

**Abstract:** One of the tasks in the operation of electric power systems is the correct functioning of the protection system and emergency automation algorithms. Instrument voltage and current transformers, operating in accordance with the laws of electromagnetism, are most often used for information support of the protection system and emergency automation algorithms. Magnetic core saturation of the specified current transformers can occur during faults. As a result, the correct functioning of the protection system and emergency automation algorithms is compromised. The consequences of current transformers saturation are mostly reflected in the main protections of network elements operating on a differential principle. This work aims to consider the analysis of current transformer saturation detection methods. The problem of identifying current transformer saturation is reduced to binary classification, and methods for solving the problem based on artificial neural networks, support vector machine, and decision tree algorithms are proposed. Computational experiments were performed, and their results were analyzed with imbalanced (dominance of the number of current transformer saturation modes over the number of modes with its normal operation) and balanced classes 0 (no current transformer saturation) and 1 (current transformer saturation).

**Keywords:** current transformer; saturation detection; protection system; artificial neural networks; support vector machine; decision tree; binary classification tasks

**MSC:** 28-02



**Citation:** Odinaev, I.; Pazderin, A.; Safaraliev, M.; Kamalov, F.; Senyuk, M.; Gubin, P.Y. Detection of Current Transformer Saturation Based on Machine Learning. *Mathematics* **2024**, *12*, 389. https://doi.org/10.3390/math12030389

Academic Editor: Jonathan Blackledge

Received: 2 January 2024
Revised: 19 January 2024
Accepted: 23 January 2024
Published: 25 January 2024



## 1. Introduction

Electromagnetic current transformers (CTs) and voltage transformers are most often used for the information support of the protection system and emergency automation (PS and EA) algorithms. Under CT core saturation conditions, the PS and EA algorithms may mismatch the requirements of selectivity, speed, reliability, and sensitivity [1]. For example, in the differential protection under internal faults with core saturation of one of the CTs, the protection may fail. In the case of an external fault in the differential protection with core saturation of one of the CTs, maloperation of the protection may occur. For clarity, Figure 1 shows the saturation of the CT with both external and internal faults in the differential protection. In the figure the currents of the protection arms are designated $I_1$ and $I_2$, respectively. From the figure, it can be seen that after an external fault for 3 ms, due to CT saturation, there is a sharp increase in the differential current $I_{Op}$ and it is equal to the restraining current $I_{Res}$. The case of $I_{Op} \approx I_{Res}$ in Figure 1 means a protection maloperation.

According to [2], under a fault with the CT core saturation, the following occurs:

– Maloperation of the PS and EA algorithms;
– Slowing down of protection algorithms;

– Reduction in the sensitivity of the PS and EA algorithms;
– False determination of the damage location.

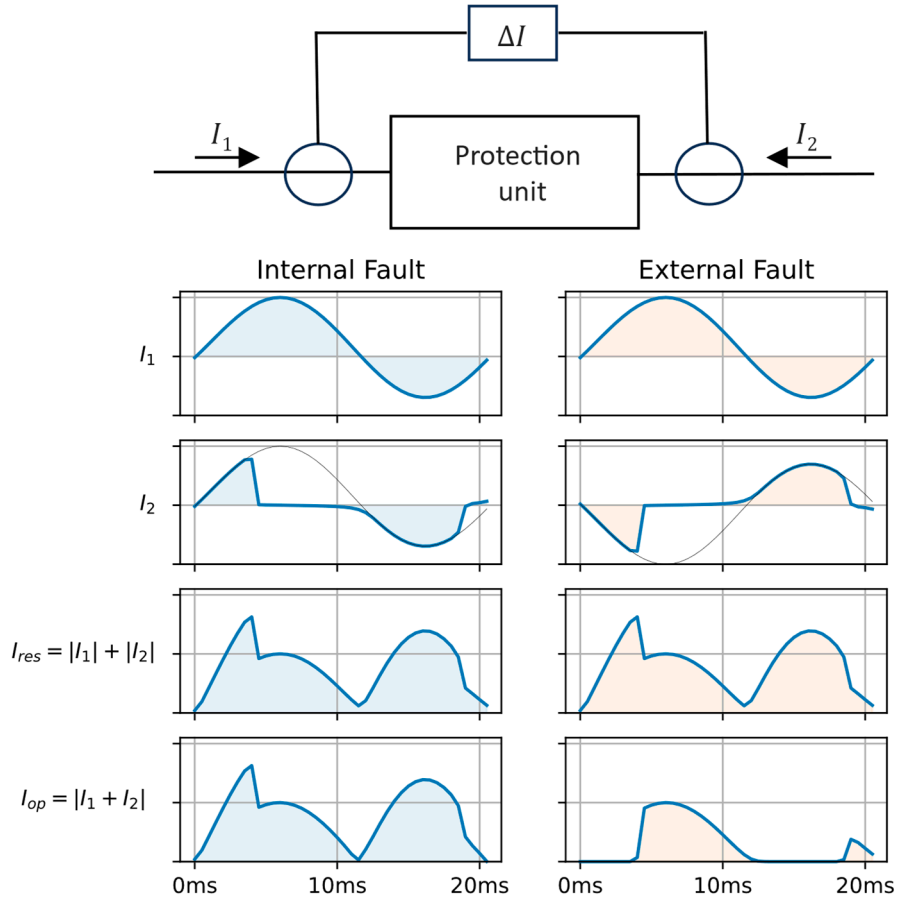


**Figure 1.** Example of internal and external faults under CT core saturation conditions.

The negative effect of the CT error under light saturation conditions on the differential principle-based protections can be compensated by restraint characteristics. However, under deep CT saturation conditions, additional restraint is used in differential protections [3]. Another way to increase the stability of PS and EA algorithms during CT saturation is to strengthen the requirements for the selection of CT, reduce the level of secondary load and "overestimate" the bending point voltage on the CT curve characteristic.

As practice shows, these ways do not fully solve the problem of CT saturation. For example, in 2018, on the 110 kV "Pyt-Yakh"—"Ugutsky" overhead power lines of the 110 kV "Ugutsky" substation (Surgut district, Khanty-Mansi Autonomous Okrug)—a fault with an unsuccessful re-closer occurred. Due to the erroneous actions of the operational personnel, a single-phase fault occurred on the same line, which led to the maloperation of the differential protection. The reason of maloperation of the protection could be the remanent flux density of the CT core established on the overhead power lines "Pyt-Yakh"—"Ugutsky"—and CT of the bus-tie switch, which appeared during the previous faults. Also, due to the CT saturation established at the 500 kV opening switchgear of the Rostov nuclear power plant, in 2014, the maloperation of the 500 kV bus bar differential protection occurred. As a result, the united power system of the south separated from the center.

Despite the causes and scale of the above-mentioned accidents, the specified CT for information support of PS and EA systems is still actively used.

This paper proposes a method for detecting CT saturation as a classification problem using artificial neural networks (ANN), support vector machine (SVM), and decision tree (DT) methods. The training of the mentioned methods during CT saturation was performed

with consideration of changes in the level of the secondary load and its components, variations in the remanent flux density and finally changes in the magnitude of the DC and AC components of the fault current.

Section 2 of this paper describes the literature review connected to the CT core saturation detection. The CT model, the essence of the ANN-, SVM-, and DT-based methods, the data generation and processing methods, and the selection of network architecture are included in Section 3. In Section 4, the conditions and results of computational experiments are presented. Sections 5 and 6 describe the conclusions and factors that will be considered in subsequent research.

## 2. Review of the CT Saturation Detection and Compensation Methods

To avoid the effect of CT saturation on the operation of differential protections for primary network elements, many heuristic approaches have been proposed [4–6]. These methods have not found wide application in practice. In addition, under deep CT saturation conditions, these methods cannot ensure the correct operation of the PS and EA systems.

Two methods have become the most common for solving the CT saturation problem: saturation detection with subsequent restoration of distorted current values [7–23] and saturation detection with subsequent blocking of the PS and EA algorithms [24–41].

The applicability of the first approach is limited by the development of theory and involves the following steps: recognition of network mode changes and their segmentation into steady-state and fault modes; dividing measurements into good and bad data obtained during the fault mode; and replacing bad data from the measured current with calculated values close to the reference current. Considering the harmonic components and noise in the fault current, the practical application of the methods from the first group is not feasible. A more detailed analysis of these methods' properties and their numerical evaluation is proposed in [42].

The methods related to the second approach have found widespread practical development due to their reliability and ease of implementation. They are based on the application of mathematical analysis methods [24–32], statistical signal processing [33–38], and the use of neural networks for classification problems [39–41].

Methods of mathematical analysis are mainly used to estimate the first derivative of the current. In the case of the CT saturation with a sharp cut of the measured current, large bursts occur in the derivative of the current. CT saturation with a sharp cut is shown in Figure 2b (the red and blue lines show the reference and measured currents, respectively). Based on these bursts, it is possible to determine at what time instant the CT core saturation occurs. Most of the methods proposed in [24–31] are based on the ideas originally presented in [32]. The advantage of them is the low computational costs of signal processing, which makes it possible to perform an analysis at the pace of the transient process. The disadvantage of these methods is their sensitivity to noise and harmonics in the measured current. To reduce noise sensitivity in [29,30], a "smoothing" Savitzky–Golay filter is used [43]. As shown in Figure 2a, in cases of CT saturation with a large reactive load, the shape of the distorted current does not contain sharp cuts. In this case, the detection of CT saturation using methods [24–32] is impossible.

The methods of statistical signal processing are based on the analysis of data extremes from one period of the measured current [33], correlation analysis of the CT secondary current with the calculated current [34], and the CT secondary currents installed on both sides of the power transformer [35]. This group also includes the analysis of the differential current form in the differential protection circuit of the power transformer [36], and the dispersion analysis of the measured current data obtained from one cycle [37] as well as the calculated values of the density [38]. Robustness to noise and the presence of harmonic components are among the main advantages of the methods in this group. The primary disadvantage is the delay in processing the measurement signal.

Furthermore, several researchers have proposed using machine learning methods to identify CT saturation [39–41]. The application of such a method is generally divided

into the following stages: data generation and collection, data preprocessing, and training and evaluation of the model. After this, the trained model can be used to solve a specific problem.

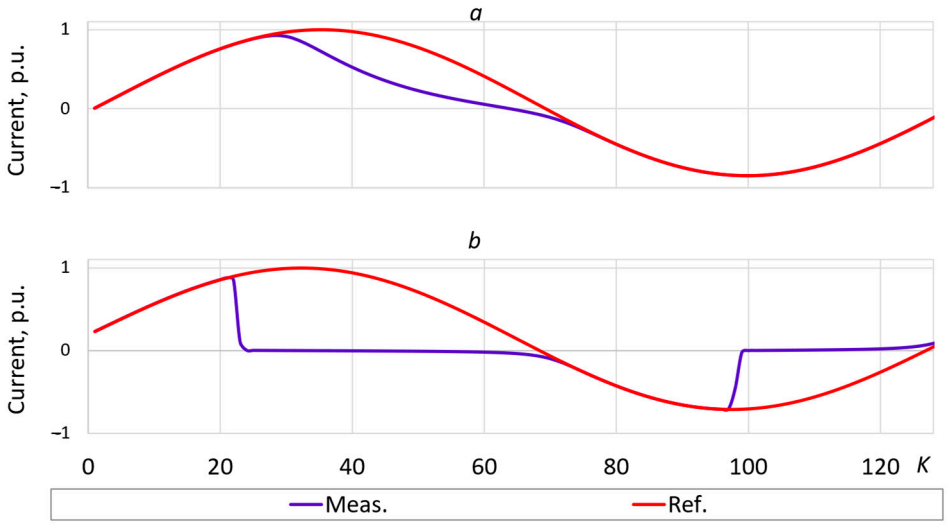


**Figure 2.** CT core saturation with smooth (**a**) and sharp (**b**) distorted currents.

To apply such methods during the preprocessing stage, data from a homogeneous process (a stable fault), lasting hundreds of milliseconds or longer, are required. In this scenario, the use of these methods, considering data preprocessing, becomes ineffective due to a significant delay.

For ease of understanding, Table 1 shows the characteristics of the considered saturation detection methods.

**Table 1.** Characteristics of CT saturation detection methods.

| Sources | Approach | Advantages/Disadvantages |
|---|---|---|
| [24–32] | mathematical analysis | (+) low computational costs, time efficiency<br>(−) sensitivity to noise and harmonics, disable to detect light CT saturation |
| [33–38] | statistical signal processing | (+) robustness to noise and harmonic components<br>(−) delay in processing the measurement signal |
| [39–41] | machine learning | (+) high flexibility and range of coverage of complex current shapes under fault conditions<br>(−) severe delay due to scaling methods, computational effort |

All these methods, as it was noted, have their advantages and disadvantages, but they can also complement each other. For example, with deep saturation, methods based on the current derivative are not able to identify CT saturation, because in the measured current, a sharp cut occurs too early—in the region near zero current values. In this case, machine learning methods and statistical approaches are more effective, since they allow a large stable section of the measured current at CT saturation to be analyzed.

## 3. Models Description and Selection

In this section, a detail description of the ANN-, SVM-, and DT-based models used for classification problem is given. The model evaluation and selection on the basis of the F-score are presented as well.

### *3.1. Description and Selection of the ANN Architecture*

The signal rate was 32 samples/cycle, and the CT saturation detection problem was identified as binary classification. Consequently, the ANN architecture with 32 inputs and 1 output is selected. Figure 3 shows the architecture of the specified ANN. The selection of

hidden layers size with the number of neurons will be after ANN modeling and evaluation. Depending on the input data, a single output neuron of network can take two states $a \in \{1, 0\}$.

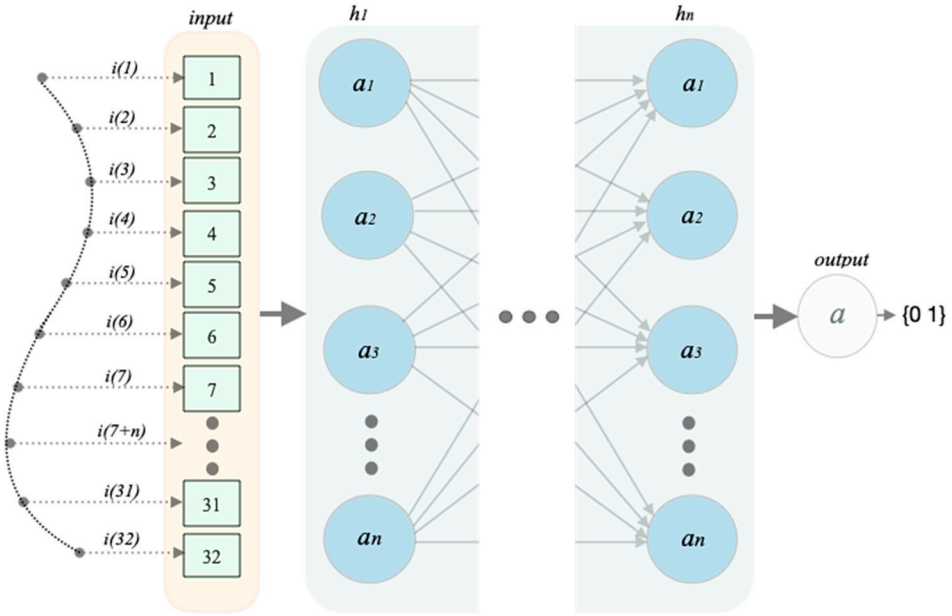


**Figure 3.** Architecture of the ANN classifier.

The loss function at the output of the ANN is selected based on the type of classification problem. Since only two classes are allocated in the CT saturation detection problem, binary classification is used. Therefore, the loss function is described as:

$$Loss = -[y \cdot log(a) + (1 - y) \cdot log(1 - a)], \quad (1)$$

where $y$ refers to true class labels, and $a$ refers to class labels at the output of the ANN.

### *3.2. SVM Description with Selecting Its Kernel*

Since SVM is one of the best representatives of the methods used for solving binary classification problems, it was selected for comparative analysis with the ANN classifier. The objective of SVM is to find the optimal hyperplane that separates the data into classes. The points closest to the hyperplane representative of different classes are called reference points. The optimal hyperplane maximizes the distance between the reference points and the hyperplane. To illustrate SVM, Figure 4 shows class data (red and blue dots) in the feature space together with separating hyperplanes in the form of straight lines. In this figure, the reference points are indicated by rhombuses. The dotted line is optimal in this case because the distance of the reference points to it is greater than the distance of the reference points to the solid line. In other words, the generalizing ability of the dashed straight line is higher than the generalizing ability of the solid straight line.

The kernel SVM algorithm can be described as:

$$a(x) = sign\left(\sum_{m=1}^{M} \lambda_m y_m K(x_m, x)\right), \quad (2)$$

where $x$, $x_m$, and $y_m$ are the classifier input point (new observation), the reference vectors (support vectors), and the corresponding true labels of the support vector classes, respectively; $\lambda_m$ represents the coefficients of the support vectors; $M$ is the total number of support vectors; and $K$ is the kernel of the SVM.

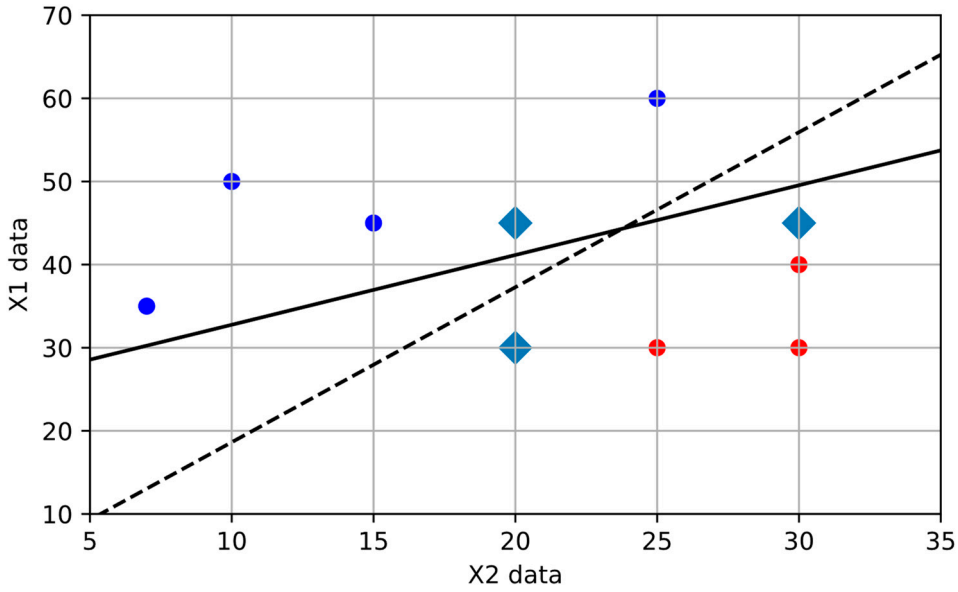


**Figure 4.** SVM visualization: solid and dotted lines are the most and least effective SVM models, respectively, red and blue points are different classes' data, respectively, and the rhombuses are reference points.

### *3.3. Decision Trees*

The DT algorithm was also chosen for a comparative analysis of the effectiveness of the methods. The algorithm utilizes nodes and leaves. The nodes divide the data into subsets in accordance with an initially selected criterion, and the leaves contain the results of the algorithm. Information entropy was used as a criterion to divide the measured values of the current in the nodes:

$$H = -\sum_{m=1}^{M} \frac{N_m}{N} log\left(\frac{N_m}{N}\right), \quad (3)$$

where $M$ is the number of classes in the original subset; $N_m$ and $N$ are the number of parameters of the $m$-th class and the total number of parameters in the subset, respectively.

Entropy is used as a measure of the heterogeneity of a subset in the context of classes. If the subset contains parameters of the same class, then the logarithm turns its argument to zero; otherwise, the entropy will be maximal. The task of entropy is to minimize its value in each subsequent subset relative to the previous one. This is how the transition is made from the root node to the final leaf. The number of transitions from the root node to the leaves determines the depth of the tree.

### *3.4. Model Evaluation and Selection*

To evaluate the model performance a set of metrics are proposed. When generating a dataset for the task of detecting CT saturation, the number of modes with saturation can significantly exceed the number of modes of normal CT operation. As a result, there is an imbalance in classes. In this case, a direct evaluation of classifier models distorts the performance indicators [44,45]. To eliminate this drawback, an error matrix with four elements is used:

- correct detection of CT normal operation—*TP*;
- correct detection of CT saturation—*TN*;
- false detection of CT normal operation—*FP*;
- false detection of CT saturation—*FN*.

Based on the elements of the confusion matrix, two indicators are calculated—precision and recall. The first one shows the proportion of true classes among the predicted classes; in other words, this indicator answers the question "how exactly does the model work?".

The second indicator determines the proportion of correctly classified modes with and without CT saturation, and it answers the question "what proportion of modes with and without CT saturation was classified correctly?". Therefore, these indicators are defined as [46]:

$$Precision = \frac{TP}{TP + FP}, \tag{4}$$

$$Recall = \frac{TP}{TP + FN}, \tag{5}$$

where *TP*, *FP*, and *FN* are the correct detection of CT normal operation, false detection of CT normal operation, and false CT saturation detection, respectively.

To integrate the above metrics, the harmonic mean—F-score—is used:

$$F = \frac{2(Precision \cdot Recall)}{Precision + Recall}. \tag{6}$$

To select the appropriate ANN-based model, the neurons number of ANN with two hidden layers was varied. The step used when changing the number of neurons was 10, with a range of 10–300. Figure 5 shows the dependency of ANN performance on the neurons number. The epoch number and learning rate were 50 and 0.7, respectively.

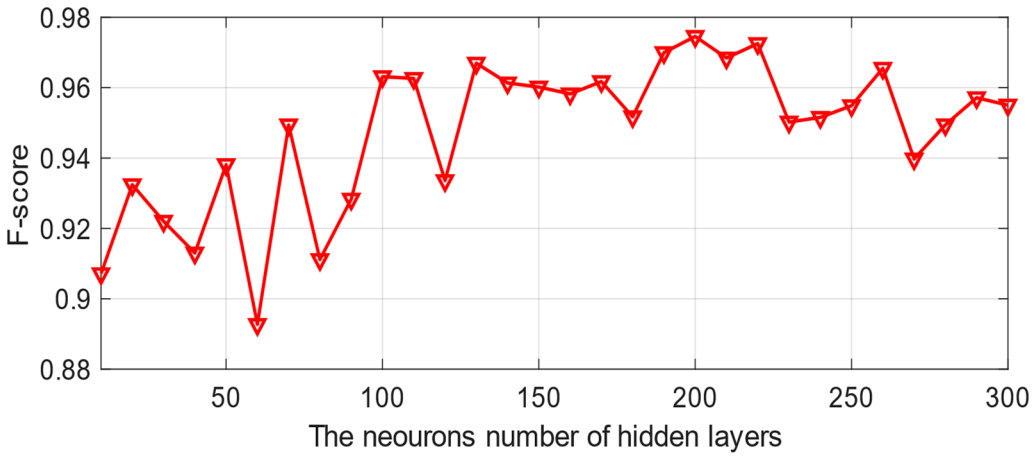


**Figure 5.** ANN performance: red triangles show the two hidden layers ANN-based models.

It can be seen from Figure 5 that the number of neurons until 200 is directly proportional to the model performance. A further increase in neuron numbers results in nonefficiency. Moreover, the higher the ANN size, the lower the calculation performance. Thus, the ANN with 32 input nodes, two hidden layers with 200 neurons each, and one output neuron was selected.

Experimental calculations showed that the most suitable kernel SVM is the third-order polynomial with a coefficient $\gamma$ = 0.5. Therefore, it will be used to solve the problem of CT saturation detection.

For the DT algorithm, according to the results of the intermediate calculations, the optimal depth of the tree is set to 5.

## 4. Description of Generating a DATASET and Data Process

In this section, the mathematical model of CT is presented. Generating a DATASET in the context of CT saturation detection is described. The set of factors effecting CT normal operation is given. The peculiarities of the window shifting effect on data properties are described as well. Then, a method of forming a class label related to the CT saturation is given. Finally, the procedure of CT saturation detection using binary classification approach is presented.

### *4.1. Generating a DATASET*

When solving the CT saturation problem using machine learning methods and artificial neural networks, the availability of accumulated statistical data, commonly referred to as a DATASET, is paramount. Typically, a DATASET contains both input (influencing factors) and output (observations) data. In the context of the CT saturation detection problem, the measured current values obtained both during CT saturation and under its normal operating conditions will be used as the input data for the ANN, SVM, and DT models.

The mathematical model of CT proposed in [47] was used for data generation. This model for single-phase CT can be described by the system:

$$\begin{cases} w_2 s \frac{d\lambda}{dt} = (R_2 + R_b) i_2 + (L_2 + L_b) \frac{i_2}{dt} \\ Hl = w_1 i_1 – w_2 i_2 \\ \lambda = f(H) \end{cases}, \quad (7)$$

where $R_b$ and $R_2$ are the active load of the secondary devices and the CT secondary winding, respectively, Ω; $L_2$ and $L_b$ are the inductance of CT the secondary winding and the load, respectively, $H$; $s$ is the cross area of the CT core, $m^2$; $l$ is the average length of the CT core magnetic line, $m$; $i_1$ and $i_2$ are the CT primary and secondary currents, respectively, $A$; $w_1$ and $w_2$ are, respectively, the number of turns of the primary and secondary windings of the CT; $\lambda$ and $B$ are the density and magnetic field strength, $T$ and A/m, respectively; $\lambda = f(B)$ is the magnetization characteristic of the CT core.

The parameters of the CT relay class included in model (7) were as follows: $s = 19.1e^{-4}$ $m^2$; $l = 90e^{-2}$ m; $w_1 = 2$ and $w_2 = 239$; $R_b = 0.98$ Ω and $R_2 = 0.48$ Ω; $L_b = 0$ and $L_2 = 3.666e^{-5}$ $H$. The CT with a non-air-gaped core is used in this paper.

The input of the model (7) was supplied with current of the two modes:

– Normal operation

$$i_1'(t) = I_{m1} sin\omega t, \quad (8)$$

– Fault

$$i_1'(t) = kI_{m1} sin(\omega t + \varphi) + I_{m2}\, e^{-\frac{(t-t0)}{T}}, \quad (9)$$

where $k$ is the scaling coefficient of the fault current; $I_{m1}$ is the amplitude of the nominal mode current; $\varphi$ is the fault angle; $I_{m2}$ and $T$ are the initial value and the attenuation time constant of the DC component of the fault current, respectively; $t_0$ is the transition moment of the mode from one characteristic to another.

It is known that the rate and depth of CT saturation are negatively affected by such factors as the amplitude of the AC component of the fault current; the initial value (the fault angle of occurrence) and the decay rate of the DC component of the fault current; the remanent flux density in the CT core; and the level and angle of CT the secondary load. Considering the variation in all factors, a series of 44,000 fault current modes were modeled:

$$N = N_1 \cdot N_2 \cdot N_3 \cdot (N_4 + N_5) = 11 \cdot 40 \cdot 10 \cdot (5 + 5) = 44000 \quad (10)$$

where $N_1$ and $N_2$ are the total number of current amplitudes and fault angles, $N_3$ is the number of remanent flux densities in CT core, and $N_4$ and $N_5$ are the number of active and reactive CT loads, respectively.

The parameters of the fault current and the remanent flux density influence only the CT saturation rate, while the level and angle of the secondary load affect both the CT saturation rate and the shape of the distorted current.

The next factor to consider is the location of saturated sections in the measured current. CT saturation can occur at any moment after a fault. To account for this, data will be fed as the input of ANN, SVM, and DT models based on the window function principle. Figure 6 illustrates an example of a shifting data window. The window width corresponds

to one cycle of the measured current. In the context of Figure 6, the sampling rate of the measured current is 16 samples/cycle. The window shifts by one packet (four samples or 5 ms). In this figure, the reference and measured currents are represented by blue and red curves, respectively. Shaded red squares on the measured current curve emphasize specific measured current samples. The required samples of the measured current for a shifting data window are marked with black rectangles at the bottom of the figure. After each shift, the oldest packet is removed from the beginning of the window (illustrated by painted red rectangles), and then four new samples from the "fresh" packet are appended at the end of the window. Vertical blue arrows indicate the end of each data window. The figure reveals that five steps are necessary for a full transition from one cycle to the next. As a result, five modes (mode1–mode5) are established for detecting CT saturation.

Thus, considering all factors, the number of input data of the DATASET is:

$$INP = N{\cdot}WndStep = 44\,000{\cdot}5 = 220\,000 \tag{11}$$

where $WndStep$ is the data window shifting step.

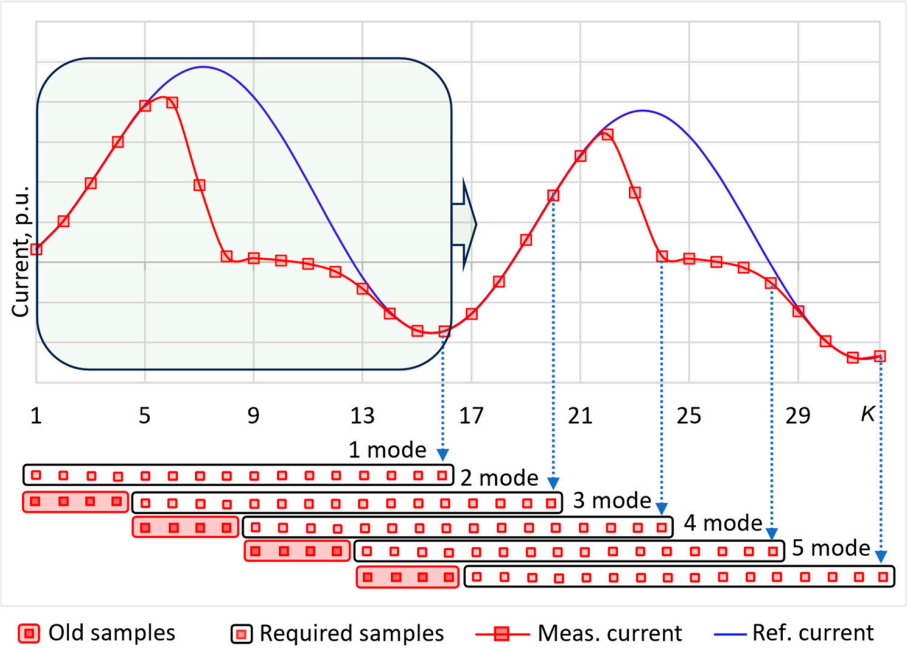


**Figure 6.** Example of a sliding window with a complete transition from the first period to the second.

When setting the CT saturation detection problem as a classification problem, two possible modes of the CT $y \in \{1, 0\}$ or $y \in \{1, -1\}$ are considered. At $y = 1$, the presence of CT saturation is established, otherwise its absence. Now, for each set of input data in the *INP*, it is necessary to provide an appropriate response at the output of the ANN, SVM, and DT models. To do this, a vector $y$ with elements of a true class label, meaning the presence or absence of CT saturation, is required. To fill the y elements, it is needed to formulate a criterion according to which the presence or absence of CT saturation is established. To this end, the CT error values-based method expressed in % is proposed.

$$Error = \frac{I_\mu}{I}100 = \frac{100}{I}\sqrt{\sum_{k=1}^{K}\left(\frac{i_1(k)}{n} - i_2(k)\right)^2}, \tag{12}$$

where $I$ and $I\mu$ are the RMS values of the CT primary and magnetizing currents reduced to the secondary side, respectively; $i_1$ and $i_2$ are the instantaneous values of the reference and measured currents; $n$ is the CT ratio; and $K$ is the sampling frequency of the signal, the amount of samples/cycle.

Next, the elements of the true class $Y$ are filled in according to the following:

$$Y = \begin{cases} 1 & if\ error\ \geq\ Th \\ 0 & if\ error < Th \end{cases}, \quad (13)$$

where $Th$ is the threshold. In the case of protection of the CT, the threshold value is set to $Th$ = 10. Depending on the CT saturation depth and the sensitivity of the PS and EA algorithms to the CT error, the threshold values can be set individually.

Signal frequency $N$ = 32 samples/period. Consequently, a DATASET is formed $X = \{\mathbf{i}_2(j),\ \mathbf{y}(j) \mid \mathbf{i}_2 = i_2(1),\ i_2(2), \ldots\ i_2(32),\ \mathbf{y} = \{0;1\}\}_{j=1}^{220\,000}$ with two classes at the output of the algorithms.

### *4.2. Scaling Methods Relatively to CT Saturation Task*

One of the key steps when using ANN, SVM, and DT classifiers is data scaling. It is worth noting that processing the data based on existing scaling methods is not possible. This is due to a short input data window, deep CT saturation, a wide range of fault current level variation, and window offset. There are fault modes whose extremums are not contained in the first window(s) of data. For clarity, Figure 7 shows two such modes. The values of currents are shown on the $Oy$ axis, and their indices are shown on the $Ox$ axis. The black and red lines highlight the reference and measured values of the currents, respectively.

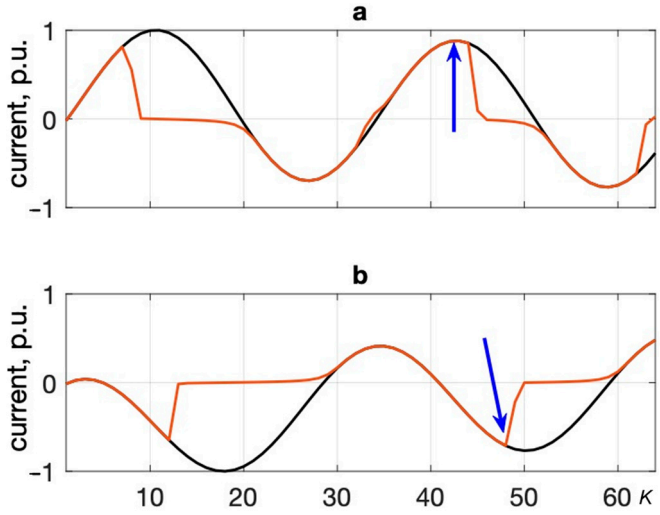


**Figure 7.** Special short-circuit modes; (**a**) displacement of the extremum from the 1st half-period to the 3rd; (**b**) displacement of the extremum from the 2nd half-period to the 4th. Red and black lines show reference and measured currents respectively, arrows show the extremum of current.

The graph in Figure 7a shows that at fault, due to the deep saturation, the extremum of the function shifted from the first half-period to the third (blue arrow). The graph in Figure 7b shows the case of a fault with an extremum of the function at the second half-period. However, due to the saturation, the extremum has shifted to the fourth half-period.

When using the Max, Min-Max, and Z-scaling methods, the scale of such data in each package will be changed when the window is shifted. In this case, with each step of the window shifting, the data scale of the same package may change until it is excluded from the window (five times). Moreover, when scaled by the Max method, near-zero current values turn into insignificant numbers. All this complicates the task and worsens the representativeness of the data. Based on the above-mentioned aspects, scaling methods will not be used at the data preprocessing stage.

The process of data processing and detection of CT saturation is shown in Figure 8.

Figure 8 shows the procedure for solving the CT saturation detection problem based on ANN, SVM, and DT classifiers. This figure contains synthesizing input data (measured

currents) based on a mathematical model of CT, forming class labels for each of the input data vector, forming a DATASET and dividing it into subsets of data, classifier modeling and evaluating, and finally classifying data (detecting CT saturation).

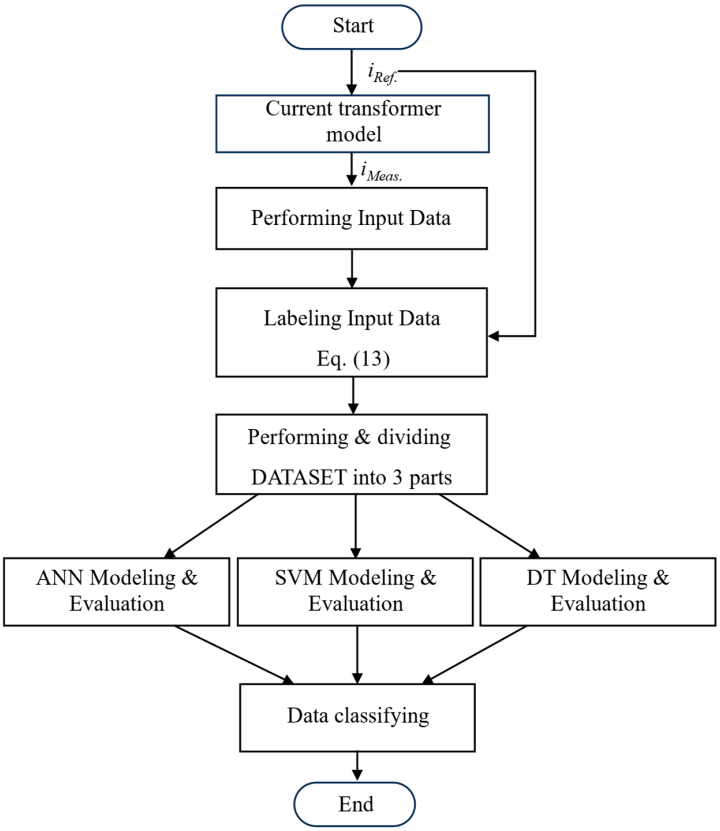


**Figure 8.** CT saturation detection process.

## 5. Computational Experiment: Results and Analysis

Before training the selected classification algorithms, it is necessary to specify their configurable parameters. It is worth noting that the stochastic gradient descent (SGD) optimizer with the momentum combination was applied to the ANN classifier during its training. The configurable parameters of ANN, SVM, and DT are shown in Table 2.

**Table 2.** Adjustable models' parameters.

| Name of the Parameter | ANN | SVM | DT |
|---|---|---|---|
| Architecture | Feedforward | - | - |
| Number of input and output nodes | 32 and 1 | 32 and 1 | - |
| Number of (hidden) layers/depth | 2 | - | 5 |
| Number of neurons in hidden layers | 200 | - | - |
| Activation functions of layers/levels | sigmoid | - | entropy |
| Distribution of initial weights | normal | - | - |
| Regularization parameter C | - | 1 | - |
| Kernel | - | 3-order polynomial | - |
| Kernel coefficient for poly, gamma | | 0.5 | - |
| DATASET size | 220,000 | | |
| Training set | 80% | 90% | 90% |
| Validation set | 10% | - | - |
| Test set | 10% | 10% | 10% |
| Learning rate | 0.07 | - | - |
| Number of iterations | 200 | 10,000 | - |
| Size of SGD minibatches | 128 | - | - |
| Decay rate $\beta$ of Momentum | 0.7 | - | - |
| Sampling rate of the signal | 32 samples/cyc. | 32 samples/cyc. | 32 samples/cyc. |
| Class labels | $y \in \{1;\ 0\}$ | $y \in \{1; -1\}$ | $y \in \{1;\ 0\}$ |

Since two classes are used in the work, it is necessary to determine the precision and recall of the model for each of them. Class 0 corresponds to normal CT operation, and Class 1 corresponds to CT saturation. The precision and recall of Class 0 are denoted as Precision_0 and Recall_0, and Class 1—Precision_1 and Recall_1, respectively.

Two experiments were carried out—with a large imbalance between classes and with balanced classes. In the case of a large imbalance, the size of the DATASET was 220,000 modes. The proportion of Class 0 and 1 in the DATASET was 5% and 95%, respectively. In the second case, to establish a balance between classes, some of the modes with CT saturation were removed from the DATASET. As a result, its size has been reduced from 220,000 to 23,066. Then, the model classifiers were re-trained and checked.

### *5.1. Experiment 1. The Imbalance between Classes 0 and 1*

The results of classifiers based on the ANN, SVM, and DT algorithms are shown in Figure 9. As shown in this figure, the accuracy and completeness of ANN for Class 0 are Precision_0 = 92.7% and Recall_0 = 97.6%, respectively. The corresponding ANN indicators for Class 1 are Precision_1 = 99.9% and Recall_1 = 99.6%.

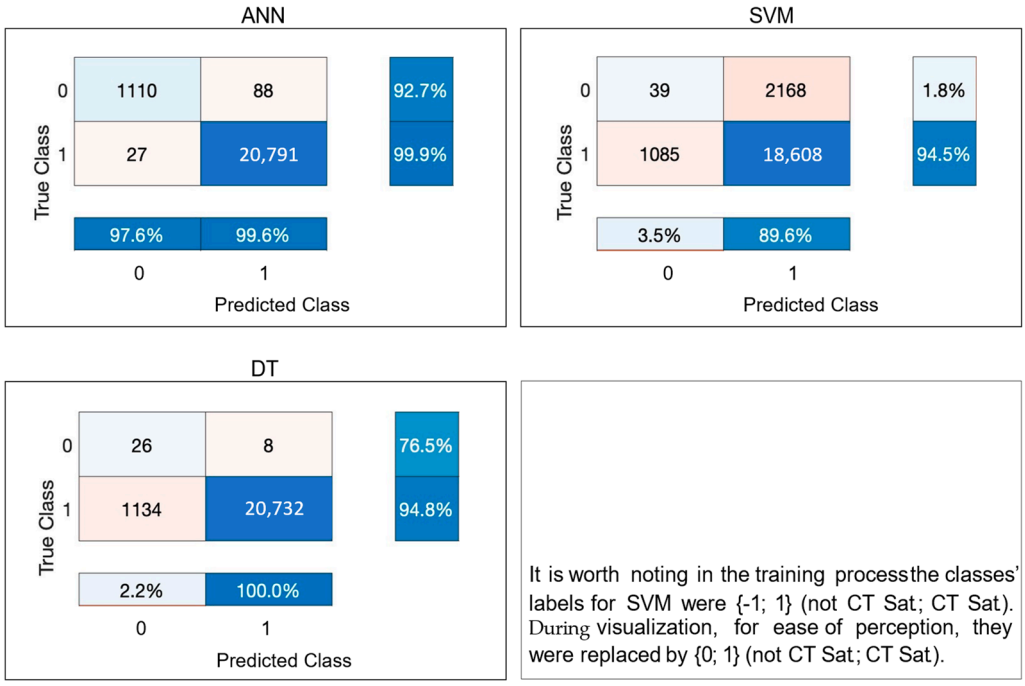


**Figure 9.** Classification results in case of imbalanced data.

The completeness and accuracy of the SVM-based classifier model for Class 0 are Precision_0 = 1.8% and Recall_0 = 3.5%, respectively. Similarly, for Class 1, Precision_1 = 94.5% and Recall_1 = 89.6%.

The efficiency of the DT-based model for Class 0 is Precision_0 = 76.5% and Recall_0 = 2.2%. For Class 1, Precision_1 = 94.8% and Recall_1 = 100%.

It is worth noting that the strong variations in classification models based on SVM and DT and the high accuracy of ANN can be caused by a large imbalance in the class itself. To test the models with balanced classes, a second computational experiment is conducted.

### *5.2. Experiment 2. Balanced Classes*

In the case of balanced class distribution, the dominance of the CT operation modes with saturation over the modes of its normal operation is eliminated. In this scenario, the quality of evaluation of the effectiveness of models increases. Figure 10 shows the results of ANN, SVM, and DT. It shows that with balanced classes, the indicators of the last two models, unlike ANN, have changed dramatically.

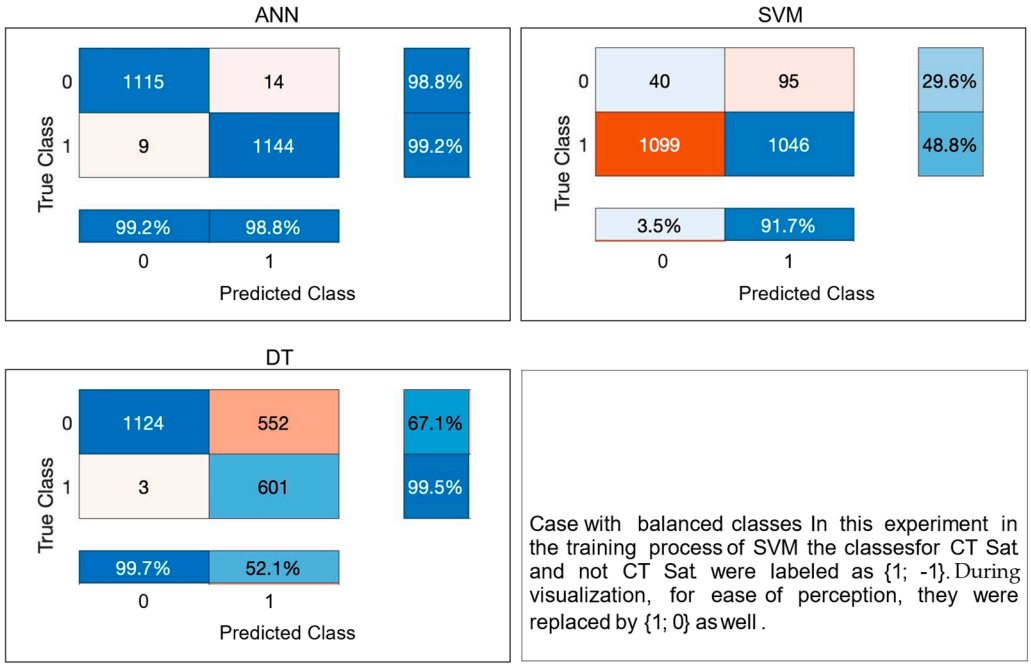


**Figure 10.** The result of classifiers with balanced classes.

In particular, the full classification for a value of 0 for the ANN-based model corresponds to Precision_0 = 98.8% and Recall_0 = 99.2%. It indicates that the ANN model for Class 1 corresponds to Precision_1 = 99.2% and Recall_1 = 98.8%.

The results based on the SVM show that for Class 0 we obtain Precision_0 = 29.6% and Recall_0 = 3.5%. Similarly, the SVM for Class 1 obtains Precision_1 = 48.8% and Recall_1 = 91.7%. As for the quality of the DT-based classifier, its results are as follows: Precision_0 = 67.1%, Recall_0 = 99.7%; Precision_1 = 99.5%, Recall_1 = 52.1%.

### *5.3. Comparison of the Results of Experiments 1 and 2*

For clarity of the discussion, the experimental results are aggregated in Table 3. The last column of the table shows the difference in the evaluation of the effectiveness of the classifiers before and after the formation of balance between classes 0 and 1.

**Table 3.** Comparative analysis of experiments 1 and 2.

| Model | Time | Metric | Experiment 1 | Experiment 2 | Difference |
|---|---|---|---|---|---|
| ANN | 14.43 ms | F-score | 99.7% | 99% | −0.7% |
| SVM | 0.035 ms | F-score | 91.96% | 63.66% | −28.3% |
| DT | 0.017 ms | F-score | 97.32% | 68.41% | −28.91% |

From the last column of Table 3, it can be seen that upon balancing the classes, the performance of the ANN-based model decreased by 0.7%. For the SVM, after establishing a class balance, the efficiency of the model deteriorated by 28.3%. The performance of the DT-based classifier with balanced classes decreased by 28.91%.

Another indicator for the models is time efficiency. To evaluate this indicator, a series of 1000 calculations was carried out to classify CT saturation modes. Then, the average value of elapsed times was obtained. In terms of time efficiency, the DT algorithm is dominant. Its time delay for classification of one fault mode is 0.017 ms. SVM takes more than twice as long as the DT algorithm (0.035 ms) to classify CT saturation for one fault mode. The ANN computational burden is turned out the most expansive—14.43 ms. However, considering the time of one cycle of AC current (20 ms), the ANN-based classifier still remains the more efficient model to solve the CT saturation problem.

The results of calculations show that among the classification methods considered, the method based on the use of ANN proved to be the most reliable and suitable for detecting CT saturation. This is due to the large number of weighting factors that increase the flexibility of the model. As for the SVM and DT methods, they turned out to be ineffective in relation to the CT saturation problem. The latter methods work effectively with small amounts of data with a small spread in distribution and range of changes.

The visual analysis of current graphs for falsely classified modes with balanced classes is interesting. To illustrate this, Figure 11 shows all 14 modes falsely classified as Class 0. The values of currents are laid on the *Oy* axis with their indices on the *Ox* axis. The blue and red lines indicate the reference and measured values of the currents, respectively. It can be seen from the graphs in Figure 11 that CT saturation occurred at a high reactive secondary load. In such cases, the shape of the distorted current does not have sharp cuts, which complicates the task of detecting CT saturation. Moreover, apart from graph *g* and *m*, the saturation depth of CT in the other graphs is low. However, the minimum error value corresponds to the graph *l* and exceeds the threshold value $T_h$ = 10, *error_l* = 10.34.

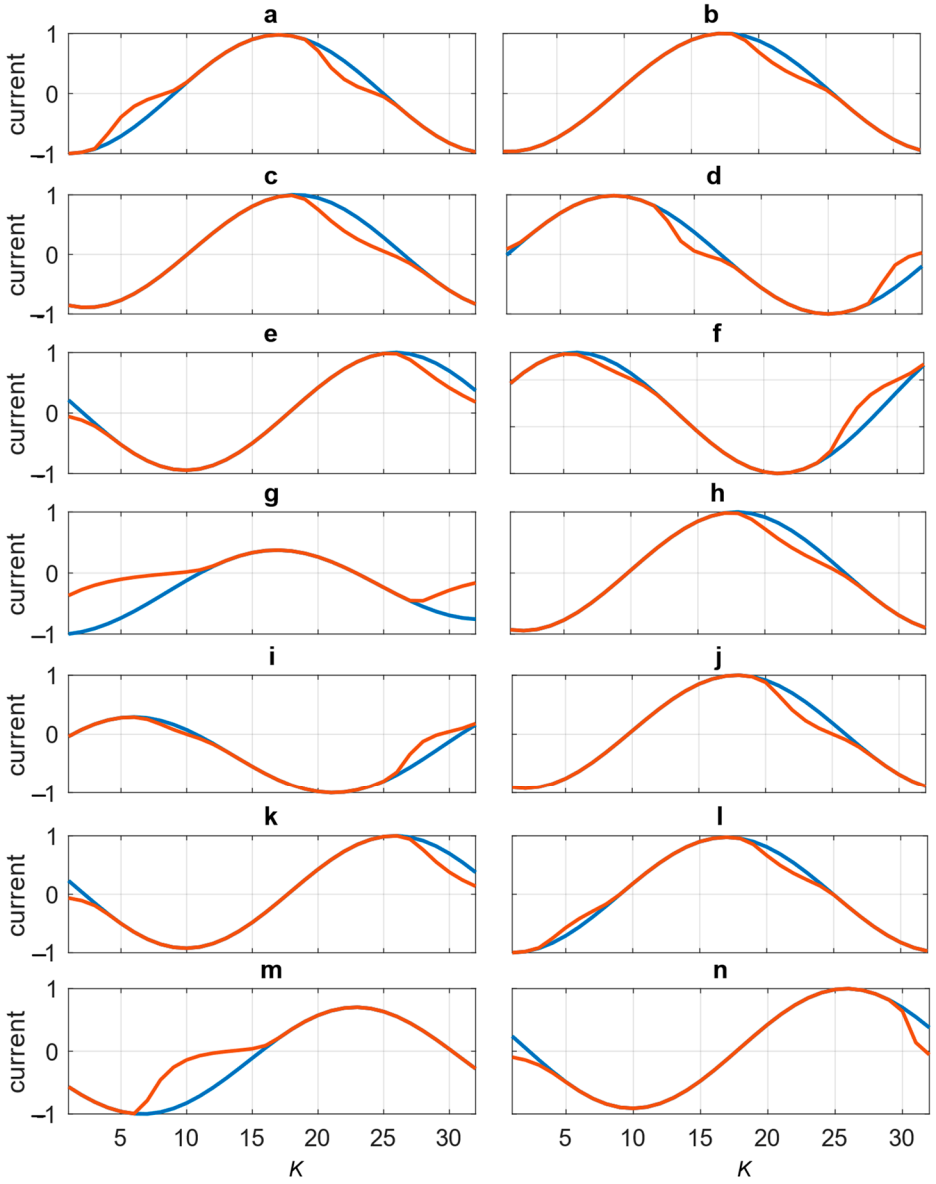


**Figure 11.** Current curves falsely classified as Class 0: graphs (**a**–**n**) are faults with different depths of CT saturation; blue and red lines show reference and measured currents, respectively.

Figure 12 shows eight of the nine modes falsely classified as Class 1. The blue and red lines highlight the reference and measured current values, respectively. The instantaneous values of currents are laid on the *Oy* axis, and their indices are laid on the *Ox* axis. It can be seen from the figure that in all modes the saturation of CT is light and it corresponds to a high reactive load of CT. The maximum total CT error for the specified parameters does not exceed the threshold $T_h$ = 10, and *error* = 9.4%. The false classification of modes as Class 0 is not as critical as in the case in Figure 12.

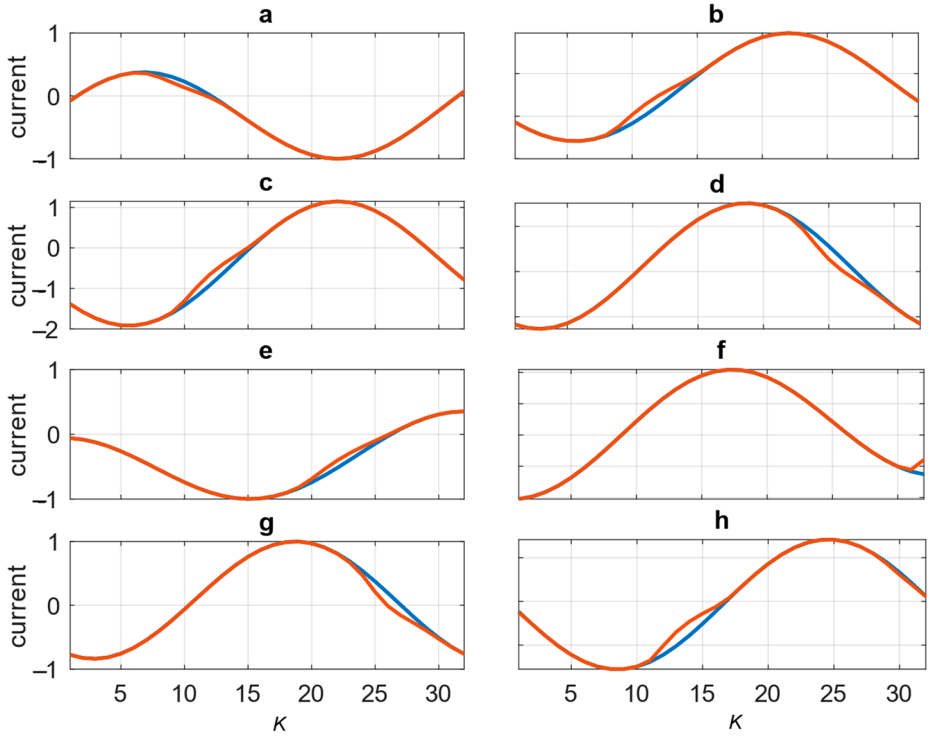


**Figure 12.** Current curves falsely classified as Class 1: graphs (**a**–**h**) are faults with different depths of CT saturation; blue and red lines show reference and measured currents, respectively.

## 6. Conclusions

In this paper, an analysis of existing methods for detecting CT saturation [48,49] has been carried out. Their advantages and disadvantages are described. The systematization of these methods is further provided in the table form. A method for detecting CT saturation using artificial neural networks, support vector machine, and decision tree algorithms for binary classification has been proposed. The properties of the algorithms are described in relation to the task of detecting CT saturation. The problem of CT saturation detection [49] is reduced to the problem of binary classification. A description of the data generation method is supplied. A method of forming a class label in relation to the task of CT saturation detection with the possibility of detuning from light saturations is proposed. Computational experiments were carried out with a large imbalance between classes 1 (CT saturation) and 0 (CT normal operation) and with their balance.

The results of the first experiment show that with a large imbalance in classes the performance of the ANN = 99.7%. This indicator for other considered models was SVM = 91.96% and DT = 97.32%. The performance comparison between ANN-based model with other ones was ANN/SVM = 1.08 and ANN/DT = 1.02 times.

In the second experiment, with balanced classes, the performance of the ANN = 99%. The performance of two last models was SVM = 63.6% and DT = 68.41%. The ANN performance relative to other models was ANN/SVM = 1.55 and ANN/DT = 1.45 times.

Thus, the ANN-based model turned out to be the most effective in the CT saturation detection problem.

In terms of time on average, the efficiency of the algorithms is as follows: $t_{ANN}$ = 14.5 ms, $t_{SVM}$ = 0.035 ms, and $t_{DT}$ = 0.017 ms.

The results demonstrate that for CT saturation detection, the ANN-based model is a more reliable and robust instrument than the SVM- and DT-based models. The robustness of ANN is shown by the fact that the model did not change its effectiveness in both balanced and imbalanced cases. Its reliability is shown by the high efficiency in both experiments.

In the second experiment, all 14 graphs of currents falsely classified as Class 0 have been visualized. The first eight of nine current graphs falsely classified as Class 1 have been shown as well. The result of the visual analysis showed that in most cases the error occurs with light CT saturation and with a large CT reactive load. In this case, the issue can be solved, for example, by lowering the *Th* threshold value at the stage of preprocessing and data preparation. It is worth noting that the case of false detection of CT saturation is not critical in relation to the case of false detection of normal CT operation, since the blocking of the PS and EA algorithms is performed.

In the future, when solving the problem of CT saturation detection, including harmonic components, the magnetizing-current inrush of a power transformer, a fluctuation in the network frequency, and noise in the magnetic circuits of the network elements is planned.

**Author Contributions:** All authors have made valuable contributions to this paper. Conceptualization, A.P. and I.O.; methodology, I.O. and M.S. (Murodbek Safaraliev); software, I.O. and P.Y.G.; validation, M.S. (Mihail Senyuk) and F.K.; formal analysis, F.K. and A.P.; investigation, A.P., M.S. (Murodbek Safaraliev), I.O. and F.K.; writing—original draft preparation, A.P., P.Y.G. and I.O.; writing—review and editing, P.Y.G., M.S. (Mihail Senyuk) and I.O.; supervision, P.Y.G., F.K., M.S. (Murodbek Safaraliev) and A.P. All authors have read and agreed to the published version of the manuscript.

**Funding:** The reported study was supported by Russian Science Foundation, research project № 23-79-01024.

**Data Availability Statement:** Data are contained within the article.

**Conflicts of Interest:** The authors declare no conflicts of interest.

## References

1. Hunt, R. Impact of CT Errors on Protective Relays-Case Studies and Analyses. *IEEE Trans. Ind. Appl.* **2012**, *48*, 52–61. [CrossRef]
2. Guerra, F.D.C.F.; Mota, W.S. Current transformer model. *IEEE Trans. Power Deliv.* **2007**, *22*, 187–194. [CrossRef]
3. Saleh, S.A.; Ozkop, E. Digital Differential Protection for $3\phi $ Solid-State Transformers. *IEEE Trans. Ind. Appl.* **2021**, *57*, 3474–3486. [CrossRef]
4. Chuanjian, W.; Qun, Y. Analysis and Countermeasure of Delay of Line Differential Protection Caused by CT Transient Saturation in Faults in Wind Farms. In Proceedings of the 2018 Chinese Automation Congress (CAC), Xi'an, China, 30 November–2 December 2018; pp. 3209–3212. [CrossRef]
5. Jun, G.; Tao, Z.; Shaofeng, H. The influence and countermeasure to transformer differential protection of CT saturation caused by external fault removal. In Proceedings of the 2008 International Conference on Electrical Machines and Systems, Wuhan, China, 17–20 October 2008; pp. 4497–4502.
6. Khanna, A. Application of ATP-EMTP in determination of optimal settings for differential protection IEDs under CT saturation. In Proceedings of the 13th International Conference on Development in Power System Protection 2016 (DPSP), Edinburgh, UK, 7–10 March 2016; pp. 1–6. [CrossRef]
7. Pan, J.; Vu, K.; Hu, Y. An efficient compensation algorithm for current transformer saturation effects. *IEEE Trans. Power Deliv.* **2004**, *19*, 1623–1628. [CrossRef]
8. Kang, Y.; Kang, S.; Park, J.; Johns, A.; Aggarwal, R. Development and hardware implementation of a compensating algorithm for the secondary current of current transformers. *IEE Proc. Electr. Power Appl.* **1996**, *143*, 41–49. [CrossRef]
9. Kang, Y.; Park, J.; Rang, S.; Johns, A.; Aggarwal, R. An algorithm for compensating secondary currents of current transformers. *IEEE Trans. Power Deliv.* **1997**, *12*, 116–124. [CrossRef]
10. Kang, Y.; Lim, U.; Kang, S.; Crossley, P. Compensation of the distortion in the secondary current caused by saturation and remanence in a CT. *IEEE Trans. Power Deliv.* **2004**, *19*, 1642–1649. [CrossRef]
11. Kang, Y.; Lim, U.; Kang, S. Compensating algorithm suitable for use with measurement-type current transformers for protection. *IEE Proc. -Gener. Transm. Distrib.* **2005**, *152*, 880–890. [CrossRef]

12. Khorashadi-Zadeh, H.; Sanaye-Pasand, M. An ANN based algorithm for correction of saturated CT secondary current. In Proceedings of the 39th International Universities Power Engineering Conference, UPEC 2004–Conference Proceedings, Bristol, UK, 6–8 September 2004; Volume 1, pp. 468–472.
13. Khorashadi-Zadeh, H.; Sanaye-Pasand, M. Correction of saturated current transformers secondary current using ANNs. *IEEE Trans. Power Deliv.* **2006**, *21*, 73–79. [CrossRef]
14. Macieira, G.; Coelho, A. Evaluation of numerical time overcurrent relay performance for current transformer saturation compensation methods. *Electr. Power Syst. Res.* **2017**, *149*, 55–64. [CrossRef]
15. Saha, M.; Izykowski, J.; Lukowicz, M.; Rosolowski, E. Application of ANN methods for instrument transformer correction in transmission line protection. In Proceedings of the 7th International Conference on Developments in Power System Protection, Amsterdam, The Netherlands, 9–12 April 2001; pp. 303–306.
16. Shi, D.; Buse, J.; Wu, Q.; Jiang, L. Fast compensation of current transformer saturation. In Proceedings of the IEEE PES Innovative Smart Grid Technologies Conference Europe, ISGT Europe, Gothenburg, Sweden, 11–13 October 2010; pp. 1–7.
17. Shi, D.; Buse, J.; Wu QGuo, C. Current transformer saturation compensation based on a partial nonlinear model. *Electr. Power Syst. Res.* **2013**, *97*, 34–40. [CrossRef]
18. Wiszniewski, A.; Rebizant, W.; Schiel, L. Correction of current transformer transient performance. *IEEE Trans. Power Deliv.* **2008**, *23*, 624–632. [CrossRef]
19. Yu, D.; Cummins, J.; Wang, Z.; Yoon, H.; Kojovic, L.; David, S. Neural network for current transformer saturation correction. In Proceedings of the 1999 IEEE Transmission and Distribution Conference, New Orleans, LA, USA, 11–16 April 1999; pp. 441–446.
20. Yu, D.; Cummins, J.; Wang, Z.; Yoon, H.; Kojovic, L. Correction of current transformer distorted secondary currents due to saturation using artificial neural networks. *IEEE Trans. Power Deliv.* **2001**, *16*, 189–194. [CrossRef]
21. Ge, B.; de Almeida, A.T.; Ferreira, F.J. Estimation of primary current in saturated current transform- er using flexible neural network. *Trans. Inst. Meas. Control* **2006**, *28*, 81–91. [CrossRef]
22. Erenturk, K. ANFIS-based compensation algorithm for cur- rent-transformer saturation effects. *IEEE Trans. Power Deliv.* **2009**, *24*, 195–201. [CrossRef]
23. Hajipour, E.; Vakilian, M.; Sanaye-Pasand, M. Current Transformer Saturation Compensation for Transformer Differential Relays. *IEEE Trans. Power Deliv.* **2015**, *30*, 2293–2302. [CrossRef]
24. Dashti, H.; Sanaye-Pasand, M.; Davarpanah, M. Current transformer saturation detectors for busbar differential protection. In Proceedings of the 2007 42nd International Universities Power Engineering Conference, Brighton, UK, 4–6 September 2007; pp. 338–343. [CrossRef]
25. Hossain, M.; Leevongwat, I.; Rastgoufard, P. A Current Transformer (CT) Saturation Detection Method for Bus Differential Protection. In Proceedings of the 2018 Clemson University Power Systems Conference (PSC), Charleston, SC, USA, 4–7 September 2018; pp. 1–5. [CrossRef]
26. Abd Allah, R.; Moussa, S.; Shehab-Eldin, E.; Hamed, M. Advanced detection and compensation scheme for current transformers saturation. In Proceedings of the 11th International Middle East Power Systems Conference, MEPCON'2006, El-Minia, Egypt, 19–21 December 2006; Volume 2, pp. 481–486.
27. Biswal, S.; Biswal, M. Detection of current transformer saturation phenomenon for secured operation of smart power network. *Electr. Power Syst. Res.* **2019**, *175*, 105926. [CrossRef]
28. Yang, L.; Zhao, J.; Crossley, P.; Li, K. A current transformer saturation detection algorithm for use in current differential protection. *Proc. Int. Conf. Electr. Control Eng. ICECE* **2010**, *3*, 3142–3146. [CrossRef]
29. Lin, G.; Song, Q.; Zhang, D.; Pan, F.; Wang, L. A hybrid method for current transformer saturation detection and compensation in smart grid. In Proceedings of the 2017 4th International Conference on Systems and Informatics (ICSAI 2017), Hangzhou, China, 11–13 November 2017; pp. 369–374.
30. Schettino, B.M.; Duque, C.A.; Silveira, P.M. Current-Transformer Saturation Detection Using Savitzky-Golay Filter. *IEEE Trans. Power Deliv.* **2016**, *31*, 1400–1401. [CrossRef]
31. Herlender, J.; Iżykowski, J.; Solak, K. Compensation of the current transformer saturation effects for transmission line fault location with impedance-differential relay. *Electr. Power Syst. Res.* **2020**, *182*, 106223. [CrossRef]
32. Kang, Y.; Kang, S.; Crossley, P. An algorithm for detecting CT saturation using the secondary current third-difference function. In Proceedings of the 2003 IEEE Bologna Power Tech Conference Proceedings, Bologna, Italy, 23–26 June 2003.
33. Bahari, S.; Hasani, T.; Sevedi, H. A New Stabilizing Method of Differential Protection Against Current Transformer Saturation Using Current Derivatives. In Proceedings of the 2020 14th International Conference on Protection and Automation of Power Systems (IPAPS), Tehran, Iran, 31 December 2019–1 January 2020; pp. 33–38. [CrossRef]
34. Behi, D.; Allahbakhshi, M.; Bagheri, A.; Tajdinian, M. A new statistical-based algorithm for CT saturation detection utilizing residual-based similarity index. In Proceedings of the 2017 25th Iranian Conference on Electrical Engineering (ICEE), Tehran, Iran, 2–4 May 2017; pp. 1072–1077. [CrossRef]
35. Etumi, A.A.A.; Anayi, F.J. The application of correlation technique in detecting internal and external faults in three-phase transformer and saturation of current transformer. *IEEE Trans. Power Deliv.* **2016**, *31*, 2131–2139. [CrossRef]
36. Zheng, T.; Huang, T.; Ma, Y.; Zhang, Z.; Liu, L. Histogram-Based Method to Avoid Maloperation of Transformer Differential Protection Due to Current- Transformer Saturation under External Faults. *IEEE Trans. Power Deliv.* **2018**, *33*, 610–619. [CrossRef]

37. Hong, C.; Haifeng, L.; Hui, J.; Jianchun, P.; Chun, H. A scheme for detection and assessment of current transformer saturation. In Proceedings of the 2017 9th International Conference on Measuring Technology and Mechatronics Automation (ICMTMA), Changsha, China, 14–15 January 2017; pp. 90–93. [CrossRef]
38. Odinaev, I.; Pazderin, A.V.; Murzin, P.V.; Tashchilin, V.A.; Samoylenko, V.O.; Ghociev, B. Detection of the initial region of the current transformer core saturation. *Renew. Energy Power Qual. J.* **2021**, *19*, 477–482. [CrossRef]
39. Ali, M.; Son, D.-H.; Kang, S.-H.; Nam, S.-R. An accurate CT saturation classification using a deep learning approach based on unsupervised feature extraction and supervised fine-tuning strategy. *Energies* **2017**, *10*, 1830. [CrossRef]
40. Key, S.; Ko, C.-S.; Song, K.-J.; Nam, S.-R. Fast Detection of Current Transformer Saturation Using Stacked Denoising Autoencoders. *Energies* **2023**, *16*, 1528. [CrossRef]
41. Rumiantsev, Y.V. Current Transformer Saturation Detection Method Based on Artificial Neural Network. *Energ. Proc. CIS High. Educ. Inst. Power Eng. Assoc.* **2023**, *66*, 233–245. [CrossRef]
42. Odinaev, I.; Gulakhmadov, A.; Murzin, P.; Tavlintsev, A.; Semenenko, S.; Kokorin, E.; Safaraliev, M.; Chen, X. Comparison of Mathematical Methods for Compensating a Current Signal under Current Transformers Saturation Conditions. *Sensors* **2021**, *21*, 7273. [CrossRef] [PubMed]
43. Schafer, R.W. What Is a Savitzky-Golay Filter? [Lecture Notes]. *EEE Signal Process. Mag.* **2011**, *28*, 111–117. [CrossRef]
44. Kamalov, F.; Leung, H.H. Deep learning regularization in imbalanced data. In Proceedings of the 2020 International Conference on Communications, Computing, Cybersecurity, and Informatics (CCCI), Sharjah, United Arab Emirates, 3–5 November 2020; pp. 1–5.
45. Elreedy, D.; Atiya, A.F.; Kamalov, F. A theoretical distribution analysis of synthetic minority oversampling technique (SMOTE) for imbalanced learning. *Mach. Learn.* **2023**, 1–21. [CrossRef]
46. Senyuk, M.; Safaraliev, M.; Kamalov, F.; Sulieman, H. Power System Transient Stability Assessment Based on Machine Learning Algorithms and Grid Topology. *Mathematics* **2023**, *11*, 525. [CrossRef]
47. Romanyuk, F.; Novash, I.; Rumiantsev, Y.; Węgierek, P. Wye-connected current transformers simplified model validation in MATLAB-Simulink. *Przegląd Elektrotechniczny* **2015**, *91*, 292–295. [CrossRef]
48. Khalyasmaa, A.I.; Senyuk, M.D.; Eroshenko, S.A. Analysis of the State of High-Voltage Current Transformers Based on Gradient Boosting on Decision Trees. *IEEE Trans. Power Deliv.* **2021**, *36*, 2154–2163. [CrossRef]
49. Senyuk, M.; Beryozkina, S.; Gubin, P.; Dmitrieva, A.; Kamalov, F.; Safaraliev, M.; Zicmane, I. Fast Algorithms for Estimating the Disturbance Inception Time in Power Systems Based on Time Series of Instantaneous Values of Current and Voltage with a High Sampling Rate. *Mathematics* **2022**, *10*, 3949. [CrossRef]